Leaky-Wave Analysis of Wideband Planar Fabry–Pérot Cavity Antennas Formed by a Thick PRS

Ahmad T. Almutawa, *Member, IEEE*, Alister Hosseini, *Member, IEEE*, David R. Jackson, *Fellow, IEEE*, and Filippo Capolino, *Senior Member, IEEE*

***Abstract*— The radiation properties of wideband Fabry–Pérot cavity (FPC) antennas have been investigated by studying the non-Foster behavior of the reflection coefficient phase of the thick partially reflective surface (PRS) forming the cavity. In order to better understand the performance of such cavities, we show for the first time that the wideband behavior can be explained via a unique dispersion characteristic of the dominant excited leaky-waves (LWs) inside such cavities. We derive new formulas that demonstrate the role of the LWs in forming wideband FPC antennas when the reflective phase of the PRS exhibits an increase with frequency within the band of operation.**

***Index Terms*— Analytic formulation, Fabry–Pérot cavity (FPC) antenna, leaky-wave antenna (LWA), partially reflective surface (PRS), wideband antenna.**

I. Introduction

PLANAR leaky-wave antennas (LWAs) have been investigated in recent years due to their simple structure and low profile nature and their ability to easily produce directive radiation [1]–[7]. Fabry–Pérot Cavity (FPC) antennas formed by thin frequency-selective surfaces (FSSs) were studied in [8]–[16]; in such cavities, the thickness of the FSS forming the partially reflective surface (PRS) was much lower than the operational wavelength, and thus the FSS was modeled as a purely reactive shunt admittance. Later, in [17], the radiation properties of FPCs formed by a thick PRS were formulated using a general two-port network to model a thick PRS, as shown in Fig. 1. Moreover, a leaky-wave analysis provided the researchers with a useful tool to study, model, and further optimize the radiation properties of such antennas [12], [13].

While being a good choice for highly directive antennas where simplicity is important [18], standard FPC antenna designs do suffer from a narrow pattern bandwidth [19], [20]. Based on previous investigations [21]–[34], a wider radiated power bandwidth can be achieved by nearly satisfying the cavity resonance condition for a wider band of frequencies by optimizing the reflection properties of the PRS. The optimized PRS exhibits a positive slope of the reflection phase when plotted versus frequency (i.e., a non-Foster type of response) over the necessary frequency band, while the magnitude of the reflection coefficient typically exhibits a drop (discussed later). Both the magnitude and phase of the PRS reflection coefficient must be optimized to avoid the splitting of the wideband response into a narrow multiband response. In general, the optimized/engineered PRS can be modeled with a single or multilayer metal/dielectric structure, e.g., a single-layer substrate with a periodic metallic layer on either side [35] or even both sides [26] and multilayer substrates with or without metallic layers [28], [29], [33].

The leaky-wave analyses in [12] and [13] (derived for thin PRS structures) are not valid for characterizing an FPC antenna with a thick PRS that has been optimized for higher bandwidth since the PRS admittance variation versus frequency was neglected due to the narrow pattern bandwidth assumption. In this paper, to address the aforementioned shortcoming, a simple and compact formula is derived to estimate the radiation intensity (defined here as the radiated

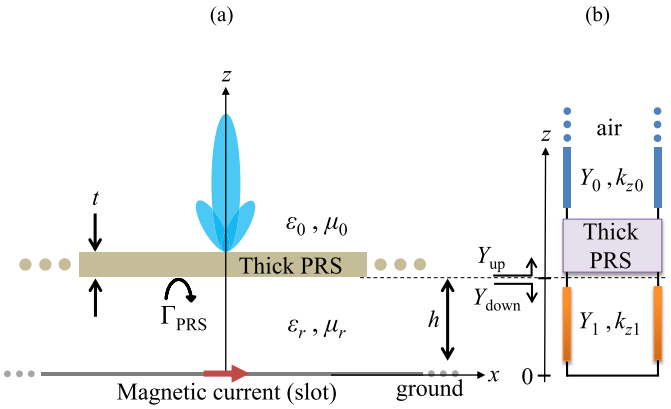

Fig. 1. (a) FPC antenna geometry using a thick PRS, excited by a slot on the ground plane. The slot is modeled as an equivalent x-directed magnetic dipole on a ground plane, and the thick PRS is modeled as a two-port network. (b) Transverse equivalent network (TEN) modeling the plane wave response of the structure in (a), as well as leaky-wave propagation on the structure.

Manuscript received July 8, 2018; revised February 9, 2019; accepted March 7, 2019. Date of publication April 15, 2019; date of current version August 12, 2019. *(Corresponding author: Ahmad T. Almutawa.)*

A. T. Almutawa and F. Capolino are with the Department of Electrical Engineering and Computer Science, University of California, Irvine, CA 92697-2625 USA (e-mail: aalmutaw@uci.edu; f.capolino@uci.edu).

A. Hosseini was with the Department of Electrical Engineering and Computer Science, University of California, Irvine, CA 92697-2625 USA. He is now with the Energous Corporation, San Jose, CA 95134 USA (e-mail: alister.hosseini@gmail.com).

D. R. Jackson is with the Department of Electrical and Computer Engineering, University of Houston, Houston, TX 77204-4005 USA (e-mail: djackson@uh.edu).

Color versions of one or more of the figures in this paper are available online at http://ieeexplore.ieee.org.

Digital Object Identifier 10.1109/TAP.2019.2911349

far-field power density multiplied by r^2 [36], [37]) of such cavities based on the leaky-wave parameters of the dominant leaky waves. To verify the accuracy of the proposed formula, a new wideband FPC antenna is designed and investigated.

A simple representation of such a wideband FPC antenna is shown generically in Fig. 1(a), formed by an infinite ground plane and a thick PRS separated with a dielectric-filled cavity of height h. In this paper and for illustration purposes, we designed a simple thick PRS constructed from an infinite dielectric layer with a relative permittivity of 6.15 backed with a thin metal surface having an infinite periodic set of circular holes. Aiming for a wideband operational bandwidth centered around 60 GHz, the PRS has been designed and optimized to maximize the broadside radiated power bandwidth from such an FPC antenna. The radiation intensity and realized gain for a finite-size structure using 10×10 unit cells excited with a rectangular slot (see Fig. 1) show a good agreement compared with the analytical results for an infinite structure, as will be demonstrated.

II. Radiation Model for Wideband Planar FPC Antenna

A planar FPC antenna formed by an electrically thick PRS is shown in Fig. 1. Here, it is assumed that the PRS, typically formed by a periodic structure, has infinite transverse extent. In order to design a wideband FPC antenna, we consider a PRS that has a reflection coefficient (from the bottom side, see Fig. 1) denoted as $\Gamma_{\rm PRS} = |\Gamma_{\rm PRS}|e^{j\phi_{\rm PRS}}$ with a phase that typically increases with frequency in a given frequency range, similar to what is discussed in [21]–[34].

The infinite horizontal (transverse) extent of the PRS allows the structure to be modeled using a transverse equivalent network (TEN) [38] as shown in Fig. 1(b). This is possible either when analyzing the antenna as a receiver, illuminated by a plane wave with transverse wavenumber k_t, or when a dipole is exciting a radiating FPC antenna, and the TEN is used to model the interaction of the planar structure with a plane wave corresponding to a spectral component of the plane-wave spectrum generated by the exciting dipole. Furthermore, the TEN is also useful when investigating the leaky modes propagating radially inside the FPC with a complex wavenumber k_t (where the radial propagation wavenumber is now a function of the angle of propagation on the structure).

For calculating the far field, reciprocity is used, which involves analyzing the FPC structure with an incident plane wave impinging on the structure, as explained in Appendix A. In this case, the transverse wavenumber k_t is real for the plane waves inside the structure. The characteristic wave admittances Y_0 and Y_1, for plane waves with either $\rm TE_z$ or $\rm TM_z$ polarization, are defined as $Y_0^{\rm TE} = k_{z0}/(\omega\mu_0)$, $Y_1^{\rm TE} = k_{z1}/(\omega\mu_0\mu_r)$ and $Y_0^{\rm TM} = \omega\varepsilon_0/k_{z0}$, $Y_1^{\rm TM} = \omega\varepsilon_0\varepsilon_r/k_{z1}$, respectively. Moreover, the vertical (longitudinal) wavenumbers in air and in the dielectric substrate region inside the FPC are $k_{z0} = \sqrt{k_0^2 - k_t^2}$ and $k_{z1} = \sqrt{k_0^2\mu_r\varepsilon_r - k_t^2}$, respectively, where k_t is the transverse wavenumber of the plane wave interacting with the FPC [38, Ch. 2] and $k_0 = \omega\sqrt{\mu_0\varepsilon_0}$ is the free space wavenumber.

We assume that the FPC antenna is fed by a slot on its ground plane, modeled as an equivalent x-directed elementary magnetic dipole ($I_m l$). Using reciprocity and the TEN, as discussed in [2], the far-field radiation from such a magnetic dipole inside the FPC, at any angle θ (Fig. 1) is related to the field H_x on the ground plane when the structure is illuminated by an incoming plane wave from the same direction θ. In the receiving case, the longitudinal wavenumbers are real and depend on the angle θ as $k_{z0} = k_0\cos\theta$ and $k_{z1} = k_0\sqrt{\mu_r\varepsilon_r - \sin^2\theta}$ [2], [12].

The assumption of cavity resonance gives a direct relation between the PRS reflection phase and frequency. The ideal reflection phase for such an FPC antenna is derived in [21] using a ray tracing model as

$$\phi_{\rm PRS}(\omega) = 2k_{z1}h + \pi(2n-1), \quad n = 0, \pm1, \pm2\ldots \tag{1}$$

FPC antennas formed by a thin PRS are usually narrowband because (1) is satisfied for a single frequency: the phase $\phi_{\rm PRS}(\omega)$ usually decreases with frequency, in accordance with Foster's theorem, while k_{z1} increases with frequency, making it possible to satisfy (1) only at one frequency.

As suggested in [21]–[34], wideband operation is achieved by properly designing the PRS to have a reflection phase closely satisfying the resonance condition (1) over a wideband frequency region for a given cavity height. For a given PRS, the cavity height that guarantees a resonance is obtained from (1) as (assuming $\theta = 0°$)

$$h = \frac{1}{2k_0\sqrt{\mu_r\varepsilon_r}}[\phi_{\rm PRS}(\omega) - \pi(2n-1)], \quad n = 0, \pm1, \pm2\ldots \tag{2}$$

We stress that because of the frequency dependence of $\phi_{\rm PRS}(\omega)$, (2) is usually satisfied only for a single frequency in the case of a thin PRS. For a wideband FPC antenna, it is desired to satisfy (2) over the bandwidth of operation. This is facilitated by having a phase $\phi_{\rm PRS}(\omega)$ that does not follow the typical Foster-like frequency dependence (that has $\partial\phi_{\rm PRS}/\partial\omega < 0$) but instead experiences a phase increase within the bandwidth of operation. A non-Foster phase response is possible since the structure radiates, and this acts as a loss mechanism for the cavity resonator.

The radiation intensity formula for such an FPC antenna has been derived using the TEN model [17] and ray tracing models [1]. The PRS reflection/admittance remain unchanged in these formulas under the assumption of highly directive FPC antennas and small value of θ at broadside [1], [8]–[10], [12]. Referring to [17] and Fig. 1(b), the TEN model has upward and downward admittances, evaluated at the bottom of the PRS, for near-broadside traveling waves as

$$Y_{\rm up} = Y_0(\hat{g} + j\hat{b}) \text{ and } Y_{\rm down} = -j\xi_r Y_0\cot(k_{z1}h)$$

where $\xi_r \equiv \sqrt{\varepsilon_r/\mu_r}$ and $Y_0 \equiv 1/\eta_0 = \sqrt{\varepsilon_0/\mu_0}$. The radiation intensity formula derived in [17], based on reciprocity, at directions near broadside for a magnetic dipole with a magnetic moment of $I_m l$ on the ground plane is

$$U(\omega,\theta) = \frac{U^+}{\sin^2(k_{z1}h)}\frac{\hat{g}}{|\xi_r\cot(k_{z1}h) - \hat{b} + j\hat{g}|^2} \tag{3}$$

where $U^+ = 2|E_0|^2\xi_r^2|I_m l|^2/\eta_0^3$, $E_0 = -j\omega\mu_0/(4\pi)$, and $k_{z1} = k_0\sqrt{\mu_r\varepsilon_r - \sin^2\theta}$. When using a ray tracing model (as originally derived in [1]), the radiation intensity near broadside is derived in terms of the PRS reflection coefficient $\Gamma_{\rm PRS}$ (a derivation is provided in Appendix A) as

$$U(\omega,\theta) = \frac{U^+}{\xi_r}\frac{1-|\Gamma_{\rm PRS}|^2}{|1-|\Gamma_{\rm PRS}|e^{j(\phi_{\rm PRS}-2k_{z1}h-\pi)}|^2}. \quad (4)$$

Although quite different in appearance, formulas (3) and (4) are algebraically equivalent and provide the same radiated power pattern for any PRS. This is proved in Appendix A.

Another method relates the radiated power from such FPC antennas to the dominant leaky wave(s) propagating radially inside the cavity structure with wavenumber $k_t = \beta - j\alpha$. For a uniform PRS formed by one or more dielectric layers, there are a pair of leaky modes, a TE_z and a TM_z leaky mode, propagating radially inside the structure, each with a slightly different value of phase and attenuation constant β and α. Maximum radiation intensity at broadside when $\beta \approx \alpha$ for each mode [12], [13].

For a periodic metallic PRS, there is often a single leaky mode of interest that is not purely TM_z or TE_z, which has a complex wavenumber that is a function of the azimuth angle of propagation ϕ on the structure (i.e., an anisotropic propagation). Assuming a magnetic dipole source oriented in the x-direction, the leaky mode becomes TM_z in the E-plane (yz plane) and TE_z in the H-plane (xz plane). For an FPC antenna optimized to radiate at broadside, the E-plane and H-plane wavenumbers of the leaky mode are usually nearly identical [3], [39]. A radiated power formula based on the leaky-wave parameters β and α for a thick optimized PRS structure would give physical insight into the wideband operation, analogous to what was done for thin PRS structures with the narrowband operation, as presented in [12] and [13]. This is the main goal of this paper.

The theory shown in this paper applies to general FPCs with arbitrary PRSs (e.g., single or multiple metal/dielectric layers [21]–[35]) that may have a frequency-dependent reflection coefficient. Practically, one of the simplest thick PRS structures that can provide a positive reflection phase slope (for increasing bandwidth) is realized from a thick dielectric substrate with a single thin FSS (e.g., 2-D periodic metal patches or holes) on the bottom surface of the substrate. This structure has been proposed in [35] to provide a dual-band FPC antenna; however, tuning the PRS parameters leads to a wideband FPC antenna response over a single band.

As an illustrative example, we consider the PRS made of a 2-D periodic FSS consisting of circular holes with diameter d in a metallic screen (copper) that is patterned on the bottom face of a dielectric layer, as shown in the PRS unit cell in Fig. 2. The unit cell of lateral size s (where $s < \lambda_0$ to avoid radiation from higher order Floquet harmonics) is made of a dielectric layer with thickness t and relative permittivity $\varepsilon_r = 6.15$, where the cavity is taken as air.

Using the finite-element method (FEM) with periodic boundary conditions implemented in Ansys HFSS, the simulated magnitude and phase of the reflection coefficient due to a normally incident plane wave impinging on the PRS ($\theta = 0°$) from below are shown in Fig. 3, where the PRS unit cell in Fig. 2 has dimensions $d = 1.35$ mm, $t = 1.27$ mm, and $s = 1.55$ mm $\approx 0.3\lambda_0$, where λ_0 is the operating free space wavelength. The PRS unit cell parameters are optimized to have a maximum -3 dB broadside power bandwidth, as will be shown in Section IV.

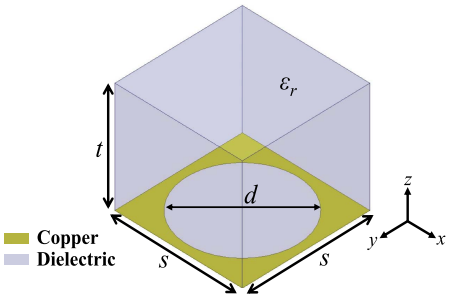

Fig. 2. Unit cell of a periodic PRS made from a dielectric layer of thickness t over a periodically patterned metallic sheet (copper) with holes of diameter d. The unit cell is periodic along x and y with period s.

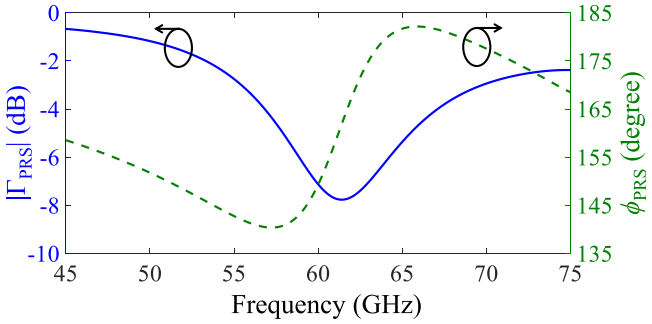

Fig. 3. Magnitude and phase of the reflection coefficient for the thick PRS shown in Fig. 2, looking up from the cavity, due to a normally incident wave (i.e., $\theta = 0°$). Note the growing phase over a frequency region, responsible for the wideband performance.

For highly directive FPC antennas and for a small range of θ near broadside, the TE/TM characteristic impedances and PRS admittances converge to their quasi TEM values at normal incidence [12], [17]. Hence, the numerical results used to validate our derived formulas throughout this paper are calculated assuming a PRS admittance and reflection coefficient that is obtained for broadside incidence where $\theta = 0°$. A numerical confirmation of this is given later (Fig. 12).

The reflection phase in Fig. 3 gradually increases with frequency in the region around 61.4 GHz, which is the desired frequency trend to achieve wideband operation in that frequency region. The study in [40] shows that the non-Foster behavior can be locally realized over a frequency region by using a negative group delay (i.e., a positive slope of the reflection phase) using a lossy resonant circuit. The non-Foster response in our structure occurs because the structure is "lossy" due to radiation [there is an air-filled half space above the PRS and an associated semi-infinite transmission line in the TEN model of Fig. 1(b)]. Although not immediately obvious, the reflection coefficient, when plotted on a Smith chart, reveals the behavior that is typical of an underdamped resonator (the trajectory with increasing frequency makes a clockwise loop that stays in the left side of the chart, with the center of the loop rotated slightly above the negative real axis).

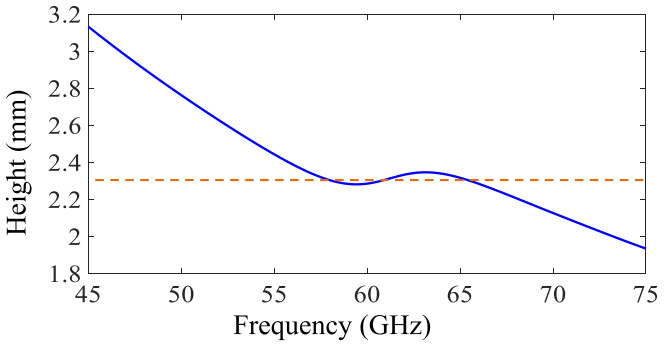

Fig. 4. Plot showing how to choose the cavity height to achieve wideband operation. The height h is calculated versus frequency using the resonance formula (2) with $n = 0$. Choosing h around 2.3 mm ensures that h nearly satisfies the ideal height requirement over as large of a band as possible.

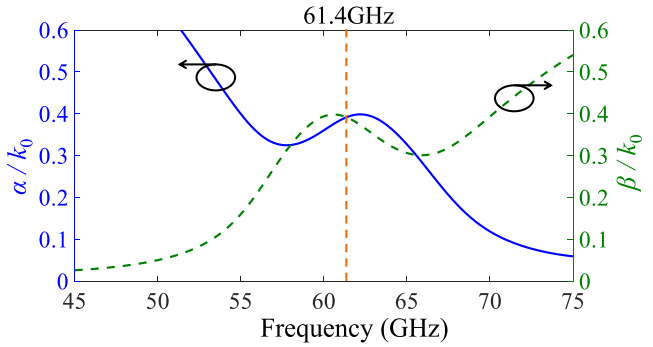

Fig. 5. Dispersion diagram for the normalized LW phase and attenuation constants for the wideband FPC antenna in Fig. 1, using the PRS shown in Fig. 2. Note the peculiar non-monotonic behavior around 61.4 GHz, nearly satisfying the relation $\hat{\beta} \approx \hat{\alpha}$ over a wide frequency band.

This explains why the magnitude of the reflection coefficient dips in the same region where the phase is increasing.

The plot in Fig. 4 shows the required FPC height h versus frequency, obtained from (2) with a reflection phase calculated at $\theta = 0°$, which ensures the ideal resonance condition at any frequency of operation. The frequency-dependent reflection coefficient in (2) is calculated via FEM. Since a fixed height has to be chosen, one can observe that the ideal height in the region around 61.4 GHz is more or less constant with respect to frequency, similar to what has been shown in [23]. [This frequency is also at the center of the non-Foster region shown in Fig. 3(a).] This means that the height choices around 2.3 mm may lead to wideband operation. Indeed, we will show that the optimum cavity height that gives a wide −3 dB radiation intensity bandwidth is around that value.

III. Leaky Waves in Wideband FPC Antennas

The radially propagating leaky mode in the xy plane, with wavenumber $k_t = \beta - j\alpha$, can be related directly to the FPC antenna geometrical parameters as well as to the far-field radiation behavior [3]–[5], [12], [13], [41], [42]. As the antenna operational bandwidth (the −3 dB radiated broadside power intensity bandwidth) significantly increases for an optimized thick PRS, the formulas derived in [12] and [13] for an FPC antenna using an electrically thin PRS (modeled as a shunt reactance in the TEN model that has a constant susceptance value vs. frequency) are not valid anymore. Aiming for a radiated power formula based on leaky-wave parameters, new more general formulas that relate the thick PRS admittance parameters (g and b in (3)) and/or PRS reflection coefficient parameters ($|\Gamma_{\text{PRS}}|$ and ϕ_{PRS} in (4)) to the leaky-wave parameters (β and α) are sought.

The leaky-wave wavenumbers in the z-direction in the region above the PRS and inside the cavity are given by [38]

$$\hat{k}_{z0} = \hat{\beta}_{z0} - j\hat{\alpha}_{z0} = \sqrt{1 - \hat{k}_t^2} \tag{5}$$

$$\hat{k}_{z1} = \hat{\beta}_{z1} - j\hat{\alpha}_{z1} = \sqrt{\mu_r \varepsilon_r - \hat{k}_t^2} \tag{6}$$

where

$$\hat{k}_t \equiv \frac{k_t}{k_0} = \frac{\beta}{k_0} - j\frac{\alpha}{k_0} = \hat{\beta} - j\hat{\alpha} \tag{7}$$

is a normalized transverse complex wavenumber of the leaky mode that propagates radially (in the xy plane), and the hat symbol indicates normalization with respect to the free space wavenumber k_0. Since here we focus on directive radiation in the broadside region, both $\hat{\alpha} \ll 1$ and $\hat{\beta} \ll 1$ [12], [43], and then (5) and (6) can be approximated as

$$\begin{aligned} \hat{\beta}_{z0} &\simeq \frac{\hat{\alpha}^2 - \hat{\beta}^2 + 2}{2} \\ \hat{\alpha}_{z0} &\simeq -\hat{\alpha}\hat{\beta} \end{aligned} \tag{8}$$

$$\begin{aligned} \hat{\beta}_{z1} &\simeq \frac{\hat{\alpha}^2 - \hat{\beta}^2 + 2n_1^2}{2n_1} \\ \hat{\alpha}_{z1} &\simeq -\frac{\hat{\alpha}\hat{\beta}}{n_1} \end{aligned} \tag{9}$$

where $n_1 = \sqrt{\varepsilon_r \mu_r}$.

The relation between the complex propagation wavenumber $\hat{k}_t = \hat{\beta} - j\hat{\alpha}$ and the frequency can be found by solving the transverse resonance equation at the point $z = h$ in the TEN model (shown in Fig. 1) for the dominant leaky mode as

$$Y_{\text{tot}}^{\text{TE/TM}}(k_t) = Y_{\text{up}}^{\text{TE/TM}}(k_t) + Y_{\text{down}}^{\text{TE/TM}}(k_t) = 0 \tag{10}$$

where

$$Y_{\text{up}}(k_t) = Y_1 \frac{1 - \Gamma_{\text{PRS}}}{1 + \Gamma_{\text{PRS}}} \tag{11}$$

$$Y_{\text{down}}(k_t) = Y_1 \frac{1 + e^{-j2k_{z1}h}}{1 - e^{-j2k_{z1}h}}. \tag{12}$$

The numerically evaluated leaky-wave wavenumber in either principal plane (E- or H-plane) is determined by solving the transverse resonance equation (10) with $h = 2.3$ mm (as discussed in Section II). The normalized values of β and α shown in Fig. 5 are approximately constant and equal to each other with a small variation in the band from 56 to 67 GHz. This gives an indication of the band for which the antenna radiates with maximum power at broadside based on the condition $\hat{\beta} \approx \hat{\alpha}$, reported in [3]–[5] and [12] for the case of narrowband LWAs.

In general, TM_z and TE_z leaky modes, corresponding to leaky-wave propagation in the E-plane and H-plane directions, respectively, have different wavenumber dispersions with frequency, since the TM_z and TE_z wave impedances are different

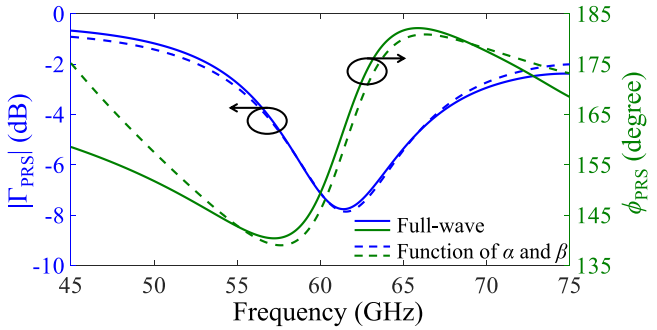

Fig. 6. Magnitude and phase of the PRS reflection coefficient. Comparison between results obtained via full-wave numerical FEM (solid line) and via the leaky-wave based formulas from (13) and (14) (dashed line). The PRS unit cell is shown in Fig. 2.

for any $k_t \neq 0$, as also shown in [3], [13], [17], [18], [34], and [43]. However, here we focus on beams pointing at broadside, and for directive FPC antennas, the transverse wavenumbers of the contributing spatial spectrum to the broadside radiation pattern are such that $|k_t| \ll k_0$ when the antenna is very directive. This means that the PRS admittance and reflection coefficient in (11) can be calculated via FEM for $k_t = 0$, i.e., under the quasi-TEM normal incidence assumption [12], [17]. This is a customary approximation in analyzing directive FPC antennas radiating at broadside that has been used also in [4], [8], [13], [17], [21], and [43]. This is consistent also with the leaky-wave parameters evaluated next, for which $\hat{\beta}^2 \ll 1$ and $\hat{\alpha}^2 \ll 1$.

The "quasi-oscillatory" dispersion behavior observed in Fig. 5 has been previously reported in [44]–[46] for the condition of $\beta \gg \alpha$ (radiated off broadside at angle $\theta > 0$) and in [34] and [47] for broadside radiation (where $\beta \approx \alpha$), where a broader power bandwidth has been demonstrated numerically.

An analytical approximation of the far-field behavior based on the leaky mode can also be derived using (4), which requires knowledge of the PRS reflection coefficient. The reflection coefficient can be obtained in terms of the leaky-wave parameters from (10) together with (11) and (12). Imposing that the imaginary part of k_{z1} to be positive for the improper leaky wave, we obtain the results

$$|\Gamma_{PRS}| = e^{-2|\hat{\alpha}_{z1}|k_0 h} \tag{13}$$

$$\phi_{PRS} = 2\hat{\beta}_{z1} k_0 h + \pi(2n-1), \quad n = 0, \pm 1, \pm 2 \ldots \tag{14}$$

Note that the normalized vertical phase and attenuation constants needed in (13) and (14) are related to the normalized phase and attenuation constants for the leaky mode via (8) and (9).

Fig. 6 shows a comparison of results for the magnitude and phase of the PRS reflection coefficient for the PRS unit cell shown in Fig. 2, comparing results from a full-wave simulation with those predicted by (13) and (14) once the leaky-wave constants β and α are numerically determined. The results are seen to be in good agreement.

From (13) and (14), an approximate relation between the leaky-wave parameters for the wideband FPC antenna can be calculated in terms of the PRS reflection coefficient as

$$\hat{\alpha} \simeq \frac{n_1}{2k_0 h} \frac{-\ln|\Gamma_{PRS}|}{\hat{\beta}} \tag{15}$$

$$\hat{\beta} \simeq \sqrt{\frac{n_1}{2k_0 h}\left(\sqrt{(\Psi^2 + \ln^2|\Gamma_{PRS}|)} - \Psi\right)} \tag{16}$$

where

$$\Psi = \phi_{PRS} - \pi(2n-1) - 2n_1 k_0 h, \quad n = 0, \pm 1, \pm 2 \ldots \tag{17}$$

Here, Ψ represents the total phase change of the wave in the cavity, composed of the phase variations during reflections from the ground [perfect electric conductor (PEC)] and PRS, and the phase change along the path length (a round trip bounce through the cavity as shown in Fig. 1). In addition, the input admittance looking up (Y_{up}) is related to the PRS reflection coefficient as

$$Y_{up}^{TE/TM} = Y_0^{TE/TM}(\hat{g} + j\hat{b}) = Y_1^{TE/TM}\frac{1-\Gamma_{PRS}}{1+\Gamma_{PRS}}. \tag{18}$$

Note that (15) predicts that the product of the normalized phase and attenuation constants is approximately a constant over a narrowband of frequency if the frequency range is small enough so that the magnitude of the PRS reflection coefficient and the electrical cavity height are approximately constant over this frequency range. This is consistent with the result for narrowband FPC antennas predicted in [9]. Note that the analysis in [12] for narrowband FPC antennas shows that

$$\hat{\alpha}\hat{\beta} \simeq \frac{1}{2} n_1^2 \tan\delta_{eff} \tag{19}$$

where $\tan\delta_{eff}$ is the effective loss tangent of the cavity that was introduced to model radiation loss, with the PRS replaced by a PEC plane so that an ideal parallel-plate waveguide filled with a lossy material is obtained. A calculation given in Appendix B shows that (19) is consistent with (15) for narrowband FPC antennas. However, the result in (15) holds even for wideband FPC antennas, while (19) does not.

Assuming the variation in the transmission line admittances in (18) with respect to frequency is negligible compared with the variation in the PRS reflection coefficient around the antenna resonance frequency, the admittances are approximated as being independent of the frequency with a fixed ratio as $Y_1^{TE/TM}/Y_0^{TE/TM} \approx \xi_r$. Using formulas (13) and (14) in (18), the normalized admittance looking up into the PRS is then

$$\hat{Y}_{up} = \hat{g} + j\hat{b} = \xi_r \frac{\sinh(2\hat{\alpha}_{z1}k_0 h) - j\sin(2\hat{\beta}_{z1}k_0 h)}{\cos(2\hat{\beta}_{z1}k_0 h) - \cosh(2\hat{\alpha}_{z1}k_0 h)}. \tag{20}$$

In the limit of small wavenumber constants ($\hat{\beta}$ and $\hat{\alpha}$), from (9) we have $\hat{\beta}_{z1} \approx 1$ and $\hat{\alpha}_{z1} \ll 1$. Hence, in the limit of small arguments of the trigonometric functions in (20), the resulting PRS admittance is then approximated as

$$\hat{Y}_{up} = \hat{g} + j\hat{b} \simeq \xi_r \frac{-\hat{\alpha}_{z1}k_0 h + j(\hat{\beta}_{z1}k_0 h - \pi)}{(\hat{\alpha}_{z1}k_0 h)^2 + (\pi - \hat{\beta}_{z1}k_0 h)^2}. \tag{21}$$

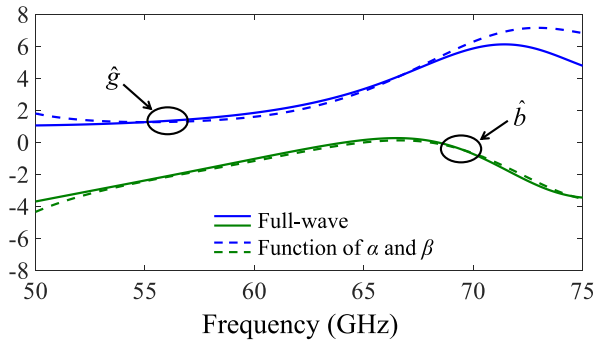

Fig. 7. Conductance (blue line) and susceptance (green line) of the PRS admittance, for the PRS shown in Fig. 2. Comparison between results obtained via full-wave numerical FEM (solid line) and the leaky-wave approximation formulas (22) and (23) (dashed line).

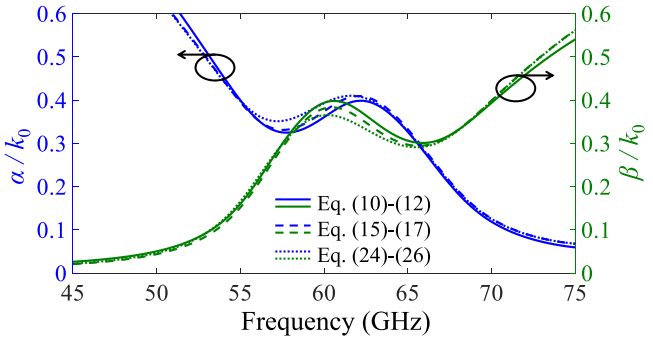

Fig. 8. Modal dispersion diagram for a leaky mode excited in a wideband FPC antenna. Comparison between the numerical solution calculated from (10)–(12) (solid line), the approximate results (15)–(17) based on the PRS reflection coefficient (dashed line), and approximate formulas (24)–(26) that are based on the PRS admittance (dotted line). The structure is the wideband FPC antenna shown in Fig. 1, with a PRS as shown in Fig. 2.

Using (9) and (21), the normalized admittance reduces to

$$\hat{g} \simeq \frac{\hat{\alpha}\hat{\beta}\xi_r n_1 k_0 h}{(\hat{\alpha}\hat{\beta}k_0 h)^2 + \left(2\pi n_1 - \left(\hat{\alpha}^2 - \hat{\beta}^2 + 2n_1^2\right)k_0 h\right)^2/4} \tag{22}$$

$$\hat{b} \simeq \frac{\xi_r n_1\left(\left(\hat{\alpha}^2 - \hat{\beta}^2 + 2n_1^2\right)k_0 h - 2\pi n_1\right)/2}{(\hat{\alpha}\hat{\beta}k_0 h)^2 + \left(2\pi n_1 - \left(\hat{\alpha}^2 - \hat{\beta}^2 + 2n_1^2\right)k_0 h\right)^2/4}. \tag{23}$$

Equations (22) and (23) tell us how the PRS is related to the wavenumber of the leaky mode; this is the inverse of (15) and (16), which tell us how the wavenumber of the leaky mode is related to the PRS. There is a good agreement between the full-wave simulation and the approximate conductance and susceptance of the PRS given by (22) and (23), as seen in Fig. 7.

In addition, another approximate relation between the leaky-wave wavenumber constants and the PRS can be derived, casting the results for the phase and attenuation constants in terms of the PRS conductance and susceptance (derivation omitted). The result is

$$\hat{\alpha} \simeq \frac{1}{\hat{g}\xi_r}\hat{\beta}(K + (\hat{g}^2 + \hat{b}^2)(\pi - n_1 k_0 h) + \xi_r \hat{b}) \tag{24}$$

$$\hat{\beta} \simeq \sqrt{\frac{n_1}{k_0 h(\hat{g}^2 + \hat{b}^2)}(K - (\hat{g}^2 + \hat{b}^2)(\pi - n_1 k_0 h) - \xi_r \hat{b})} \tag{25}$$

where

$$K = \sqrt{(\hat{g}^2 + \hat{b}^2)(\hat{g}^2(\pi - n_1 k_0 h)^2 + (\hat{b}\,(\pi - n_1 k_0 h) + \xi_r)^2)}. \tag{26}$$

Fig. 8 shows the comparison of the leaky-wave parameters: 1) the numerical solution from (10); 2) the approximate result that comes from the PRS reflection coefficient in (15)–(17); and 3) the result that comes from the PRS admittance in (24)–(26). The agreement between all three approaches is seen to be good, with the approximate result from (15)–(17) being a bit more accurate than the approximate result from (24)–(26).

IV. Radiation Pattern of Wideband FPC Antennas as a Function of Leaky-Wave Parameters

Considering wideband FPC antennas formed by a thick PRS, the leaky mode propagating radially in the *xy* plane can be related directly to the geometrical parameters (as derived in Section III). Power formula (3) has been derived for a lossless PRS and the assumption that the angle θ is small (radiation near broadside), which is appropriate for highly directive antennas. Using Taylor approximations for the trigonometric functions with an argument around π, namely, $\sin(k_{z1}h) \simeq -(k_{z1}h - \pi)$ and $\cot(k_{z1}h) \simeq 1/(k_{z1}h - \pi)$, the power formula can be further approximated as

$$U(\omega, \theta) \simeq \frac{U^+}{(k_{z1}h - \pi)^2}\left(\frac{\hat{g}}{\hat{g}^2 + (\hat{b} - \xi_r/(k_{z1}h - \pi))^2}\right). \tag{27}$$

In addition, the longitudinal wavenumber inside the cavity is approximated as $k_{z1} \simeq k_0(n_1 - (\sin^2\theta)/(2n_1))$. Using formulas (22) and (23) in (27) then reduces (27), after some algebraic manipulation, to

$$U(\omega, \theta) \simeq \frac{4n_1 U^+}{\xi_r k_0 h}\left(\frac{\hat{\alpha}\hat{\beta}}{4\hat{\alpha}^2\hat{\beta}^2 + (\hat{\alpha}^2 - \hat{\beta}^2 + \sin^2\theta)^2}\right). \tag{28}$$

This formula is valid for any FPC antenna with an arbitrary thick PRS (e.g., formed by single or multilayer metal/dielectric structures) where the normalized leaky-wave constants ($\hat{\beta}$ and $\hat{\alpha}$) are much less than unity, resulting in a highly directive antenna. Although the normalized phase and attenuation constants appear independently in (28), they are related by (15), and hence (28) only applies for an FPC leaky-wave antenna structure. However, it can be shown that the far-field power pattern for an arbitrary bi-directional 1-D LWA has the form

$$U(\omega, \theta) \simeq |A(\omega)|^2\left(\frac{\hat{\beta}^2 + \hat{\alpha}^2}{4\hat{\alpha}^2\hat{\beta}^2 + (\hat{\alpha}^2 - \hat{\beta}^2 + \sin^2\theta)^2}\right) \tag{29}$$

where $A(\omega)$ is an excitation coefficient that is proportional to the amplitude of the leaky mode. Comparing (28) and (29), it is seen that at any given fixed frequency, for which the normalized wavenumbers are fixed, the shape of the two patterns is identical, as expected.

Assuming a small broadside beamwidth, formula (28) predicts angular beam splitting when $\hat{\beta}$ becomes larger than $\hat{\alpha}$, as shown in [12]. From (28), the beam maximum is at

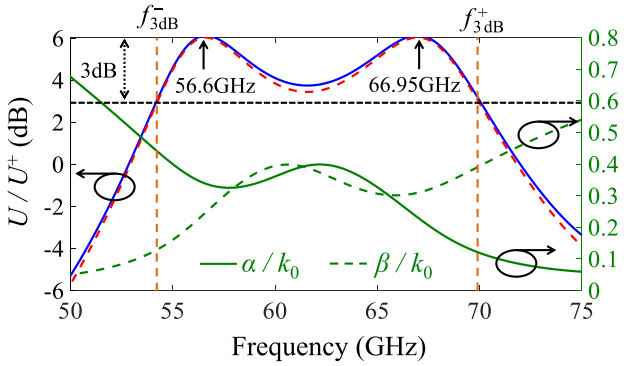

Fig. 9. Comparison of the normalized radiation intensity $U(\omega, \theta = 0°)/U^+$, radiated at broadside, estimated by the exact formula (3) from applying reciprocity (solid line) and by the leaky-wave formula (30) (red dashed line). The plot also shows the normalized leaky-wave phase and attenuation constants versus frequency for the wideband FPC in Fig. 1. The FPC has infinite transverse extent and the unit cell of the PRS is shown in Fig. 2.

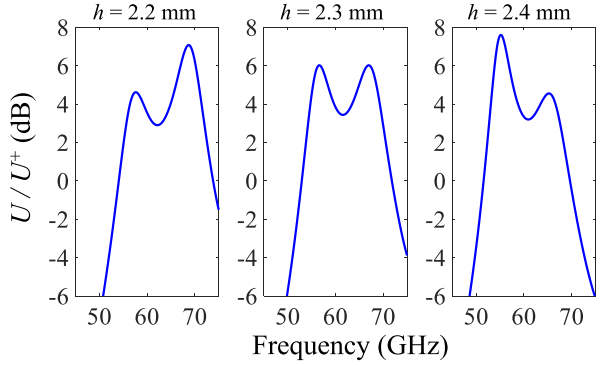

Fig. 10. Comparison of the normalized radiation intensity radiated at broadside, calculated by the leaky-wave formula (30) for three different cavity heights. Note that the value $h = 2.3$ mm is the best, since the dip at the center is not lower than -3 dB compared to the maximum.

broadside ($\theta = 0°$) when $\hat{\beta} < \hat{\alpha}$ and at an angle of $\theta = \sin^{-1}(\sqrt{\hat{\beta}^2 - \hat{\alpha}^2})$ when $\hat{\beta} > \hat{\alpha}$. At broadside, where $\theta = 0°$, (28) reduces to

$$U(\omega, 0) \simeq \frac{4n_1 U^+}{\xi_r k_0 h}\left(\frac{\hat{\alpha}\hat{\beta}}{(\hat{\alpha}^2 + \hat{\beta}^2)^2}\right). \tag{30}$$

Fig. 9 shows a good match between the normalized broadside radiation intensity versus frequency, from the exact formula (3) based on reciprocity and from the leaky-wave approximate formula (30). The good agreement in Fig. 9 demonstrates that the far-field pattern is determined by the leaky-wave parameters $\hat{\beta}$ and $\hat{\alpha}$ over the entire operating bandwidth. It is seen that the frequency range where the phase and attenuation constants are almost equal to each other covers most of the -3 dB power bandwidth region (between about 54 and 70 GHz). However, both the phase and attenuation constants show an oscillating behavior within the bandwidth because of the broadband nature of the FPC antenna, as opposed to narrowband FPC antennas where the phase and attenuation constants are monotonic and equal only at the optimum frequency of maximum broadside radiation [2]. This result verifies the correlation between the radiated power pattern and the wavenumber of the leaky mode for the wideband FPC antenna structure.

Referring to Fig. 4, the resonant FPC height versus frequency appears to have a quasi-oscillating behavior around $h = 2.3$ mm in a wideband frequency region, indicating that $h = 2.3$ mm is the best choice. This is further demonstrated in Fig. 10 that shows a parametric analysis on the broadside radiated power intensity (30) versus frequency for different cavity heights. Fig. 10 shows how the cavity height has to be chosen properly to ensure the largest broadside power bandwidth.

The optimum choice of the cavity height (see Figs. 4 and 10) will give the maximum -3 dB power bandwidth centered around 61.4 GHz. From Fig. 9, the -3 dB radiation intensity bandwidth is approximately 15.8 GHz, which is much larger than that of the narrowband cases in [9], [12], and [17]. Formula (30) holds for FPCs with any type of thick PRS formed from single or multiple layers of metal and/or dielectric.

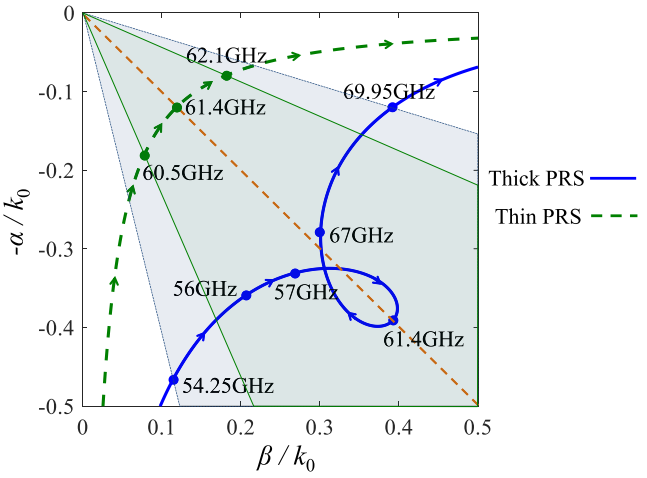

Fig. 11. Wavenumber trajectory (solid line) in the complex $k_t/k_0 = \hat{\beta} - j\hat{\alpha}$ plane for the LW in the wideband FPC antenna structure shown in Fig. 1 constructed from the PRS shown in Fig. 2. Solutions found based on formulas (10)–(12). This trajectory is compared with the conventional hyperbolic trajectory (dashed line) for the mode in a narrowband FPC antenna structure. In both designs, the center frequency is around 61.4 GHz. The shaded area represents the -3 dB region of the power bandwidth for both cases.

The results in Fig. 11 show the trajectories (varying frequency) of the normalized modal wavenumber in the complex $k_t/k_0 = \hat{\beta} - j\hat{\alpha}$ plane, of the leaky mode propagating in the wideband FPC antenna formed by the thick PRS and the leaky mode in a narrowband FPC antenna formed by a thin PRS (using a thin metallic sheet with periodic circular holes as used in the thick PRS shown in Fig. 2). The design of the narrowband FPC operates at the same central frequency and has the same cavity properties and height as in the thick PRS case, except with a smaller unit cell size $s = 1.42$ mm and a circular hole diameter $d = 1.22$ mm, which results in a higher directivity of $D_{\max} \approx 19.3$ dB and a broadside power bandwidth of 2.86%. Nevertheless, this comparison is used to show the dramatic difference in dispersion behavior.

Both the wideband and narrowband antennas radiate around the central frequency of 61.4 GHz. By varying frequency, the complex wavenumber describing the leaky mode in the wideband FPC antenna makes a loop trajectory causing $\beta = \alpha$ to occur at three different frequencies (where the blue solid

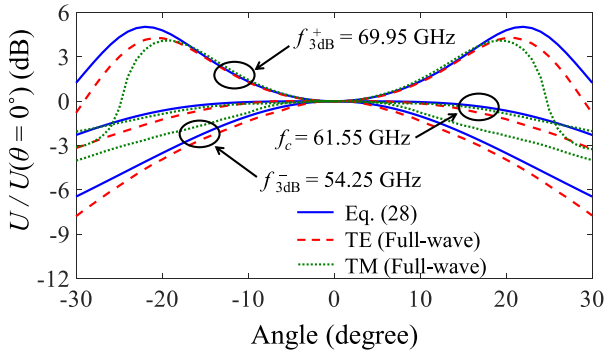

Fig. 12. Normalized angular radiation intensity [i.e., $U/U(\theta = 0°)$] as a function of angle θ for three different frequencies for the FPC with an infinite extent and a unit cell shown in Fig. 2. The plot shows a comparison between the result provided by leaky-wave formula (28) and the ones from full-wave simulation for the E- and H-planes. The approximate LW formula is accurate for small angles but it starts to deviate from the full-wave results as the angle increases.

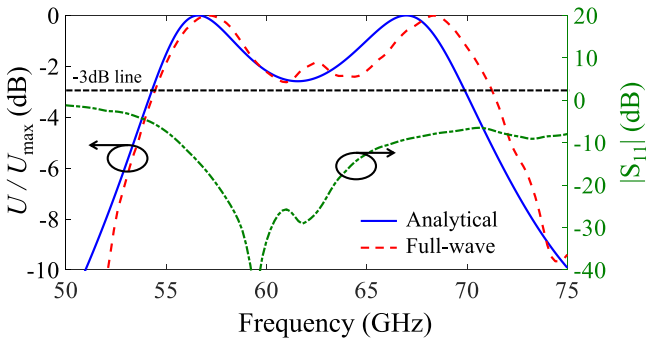

Fig. 13. Analytical results versus full-wave simulation for the normalized broadside power intensity of the wideband structure in Fig. 1. The magnitude of the reflection coefficient at the feed port is also shown. The analytical solution assumes that the antenna is of infinite extent. The full-wave simulations model the PRS made of 10×10 unit cells for the structure shown in Fig. 2.

curve crosses the red dashed line for the thick PRS seen in Fig. 11). For a narrowband FPC antenna with a thin PRS, the normalized wavenumber obeys an approximate (hyperbolic) relationship (green dashed curve in Fig. 11) where $\hat{\alpha}\hat{\beta} =$ constant, as originally shown in [3] and [12]. In comparison, the wavenumber trajectory for a thick PRS exhibits a more complicated behavior around the PRS resonance frequency, resulting in a wide frequency range of $\hat{\alpha}$ and $\hat{\beta}$ that are close to each other, as also shown in Fig. 9.

Fig. 12 shows the angular radiation intensity pattern from (28) along with the simulated far-field pattern in the E-plane (i.e., yz plane, $\phi = 90°$) and H-plane (i.e., xz plane, $\phi = 0°$) of the structure versus frequency, with results shown at 61.55 GHz (the center of the -3 dB band) as well as at the upper ($f = f^{+}_{3dB} = 69.95$ GHz) and lower ($f = f^{-}_{3dB} = 54.25$ GHz) -3 dB bandwidth limits. The patterns from (28) are obtained under the assumption of constant PRS reflection/admittance parameters calculated for $\theta = 0°$ and under the assumption of a quasi-TEM characteristic impedance (i.e., the TE and TM characteristic impedances in the TEN are approximated with that of a TEM wave at normal incidence). The full-wave E- and H-plane patterns are numerically calculated using periodic boundary conditions implemented in a full-wave simulation for a single unit cell (Fig. 2) on top of an air cavity of height $h = 2.3$ mm. With a plane wave impinging on the structure from above, the magnetic field is been calculated at the magnetic dipole source location on the ground plane for a TE_z and TM_z polarized wave separately, varying the angle of incidence of the plane wave (Using TM_z incidence models correctly the E-plane pattern, while using TE_z incidence models correctly the H-plane pattern, accounting for the angle variation of the line impedances in the TEN.) A close agreement is observed between the analytical [i.e., predicted from (28)] and the infinite full-wave simulated for both E- and H-planes, especially within the -3 dB beamwidth region. Note that the frequency for which the normalized phase and attenuation constants are equal (61.55 GHz) is not the frequency of the narrowest beam. This is consistent with the results from [12], which show that for thin PRS structures the narrowest beam occurs when the frequency is lowered slightly from the $\beta = \alpha$ condition.

V. Results for a Practical, Finite Size, and Wideband FPC Antenna

We investigate the performance of a wideband FPC antenna formed with a thick PRS and finite transverse dimensions ($10\times$ 10 unit cells). The FPC has an air-filled cavity with a height of 2.3 mm (as discussed in Section II). The PRS unit cell is square, the one proposed in Section II, Fig. 2, with dimensions of 15.5 mm $\times$ 15.5 mm, over a ground plane. Simulations are carried out using the FEM implemented in Ansys HFSS. The PRS substrate is chosen to be Rogers RT/duroid 6006 having a relative permittivity of $\varepsilon_r = 6.15$ and a loss tangent of $\tan\delta = 0.0019$ with a dielectric thickness of $t = 1.27$ mm and a copper cladding thickness of 18 μm. The antenna is fed by a rectangular wave port (i.e., a 2.25 mm $\times$ 0.5 mm slot in the middle of the ground plane) where the electric field is polarized along the y-axis. The truncated antenna dimensions are chosen so that the radiation efficiency is more than 90% over the entire -3 dB power bandwidth. The difference of the field intensity from the center (i.e., the source location) to the edge of the structure (and normalized to the field intensity at the center) is calculated as $1-\exp(-2\alpha L)$ [48], where α is the leaky-wave attenuation constant in the transverse plane and L is the length from the feeding location to the edge of the FPC structure. In our case (where $L = 7.75$ mm), the normalized field-intensity difference at the upper and lower limits of the -3 dB power bandwidth is 93.63% and 99.95%, respectively.

The simulated broadside radiation power intensity of the finite-extent FPC structure versus frequency is presented in Fig. 13, along with the analytical result using (30) that pertains to an FPC structure with infinite extent. We also plot the magnitude of the reflection coefficient associated with the waveguide feed port, whose impedance is calculated as $2P/|I|^2$ where P is the complex power passing through the port and I is the current flowing into the structure [49]. Despite the small shift in frequency due to the truncated structure and/or material and simulation inaccuracy, an overall agreement is

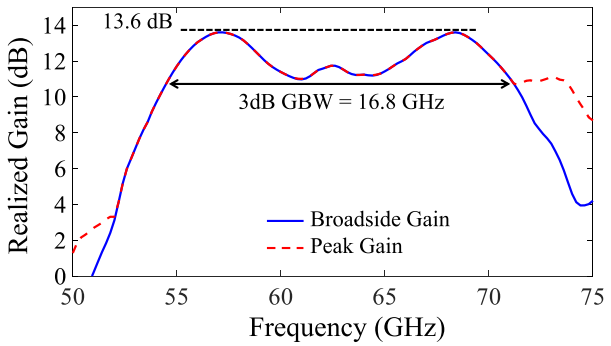

Fig. 14. Realized broadside gain and peak gain vs. frequency from simulation, for the wideband structure in Fig. 1. The PRS is made from 10×10 unit cells of the structure shown in Fig. 2.

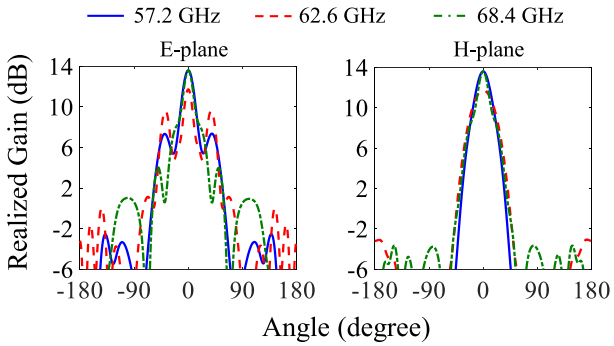

Fig. 15. Full-wave simulated realized gain in the E- and H-planes versus angle θ for the proposed structure having 10×10 unit cells as shown in Fig. 2 at 57.2, 62.6, and 68.4 GHz.

seen between the analytical and simulated results over the desired -3 dB radiated power bandwidth.

The maximum directivity obtained from the full-wave simulation of the proposed finite-size FPC antenna at broadside is 27.79 (i.e., 14.44 dBi). The -3 dB broadside power bandwidth (PBW) calculated from the results in Fig. 13 is PBW $=$ 15.7 GHz (25.6%). Based on these results, a figure of merit (FoM) defined by the product of maximum directivity and the -3 dB broadside power bandwidth is FoM $=$ (27.79) $\times$ (0.256) $=$ 7.11. The maximum bound for the FoM for a narrowband FPC antenna with a very thin planar PRS is given by $2.48/\varepsilon_r$ [4], [13]. (The bound for the FoM for narrowband FPC antennas was introduced in [13], where there was typo, corrected in [4].) Therefore, for this particular wideband FPC antenna, the FoM exceeds the thin PRS bound by a factor of 2.87.

In addition, the broadside realized gain $G = 4\pi U/P_{\text{input}}$ versus frequency obtained from the simulation is presented in Fig. 14. The broadside gain is calculated using $U(0°)$, whereas the maximum gain is calculated with the maximum value of $U(\theta)$ (see Fig. 12). This shows a maximum gain of 13.6 dB (gain of 22.9) and a -3 dB gain bandwidth of 16.8 GHz (27.4%). The simulated radiation efficiency (defined as the ratio of the radiated power in all direction over the accepted power) is larger than 94% over the -3 dB broadside gain bandwidth, while the aperture efficiency varies between 10% and 20% in the same band. This low aperture efficiency is related to a high leakage (attenuation) constant α (causing the aperture field over the PRS to be concentrated above the feeding location, as has been demonstrated in [50]). The aperture field exponentially decays away from the center toward the edges because of the attenuation constant. Further studies related to the aperture efficiency and truncation effects are reported in [51] and [52]. The study in [52] demonstrated a high gain antenna with wideband radiation from a small FPC-based antenna, where in this case, the radiated power comes also from the edges in addition to the leaky-wave contribution analogous to the one in this paper.

The simulated radiation patterns at the two frequency peaks of 57.2 and 68.4 GHz in Fig. 14, along with that at the center of the band at 62.6 GHz, are shown in Fig. 15, for both the E- and H-planes. We observe from this truncated structure similar beam patterns near broadside through the bandwidth region in the E- and H-planes. The gain has dropped at the center frequency by about 2 dB compared with the other two frequencies. This is consistent with the result shown in Figs. 9 and 13, and Fig. 10 for the $h = 2.3$ mm case.

The patterns in the E- and H-planes in Fig. 15 are narrower than the ones calculated for the FPC with infinite extent, shown in Fig. 12. This could possibly be due to reflections from the edges of the truncated structure, which may perhaps serve to narrow the main beam. For the same reason, the E-plane patterns in Fig. 15 are narrower than the H-plane patterns, whereas for the infinite structure, they are essentially equal (see the TE and TM patterns in Fig. 12). Furthermore, in this rather small FPC of finite extent, some radiation may also come from the edges.

VI. Conclusion

New formulas for wideband FPC antennas have been presented, based on representing the radiation performance of the FPC antenna in terms of leaky waves excited in the FPC. These new formulas for wideband FPC antennas significantly extend previous works that were focused only on narrowband FPC antennas with a planar and electrically thin PRS. The new derived leaky-wave-based power formula is applicable to the description of any FPC made of an electrically thick PRS formed from a combination of multiconductor and/or multidielectric layers. A good agreement was observed in all studied cases between the results based on the new analytic formulas and the results from full-wave simulations.

A full-wave simulation of a practical finite-size (i.e., truncated) FPC antenna structure was also performed, in order to show that the derived formulas predict the radiation features of practical FPC antennas even for moderate gains. The FPC antenna with a truncated ground plane and PRS has a directivity of about 14.4 dBi and a radiation intensity bandwidth of about 25.6%. The directivity-bandwidth figure of merit is 2.87 times larger than the best obtainable with planar and thin PRS structures. The leaky-wave analysis shown here is even more accurate for high directivity FPC antennas, where the leaky waves have a small attenuation constant.

This paper also demonstrates that a knowledge of the leaky-mode wavenumber is sufficient to predict the wideband behavior of a radiating FPC antenna (previous papers focused on the same predictions for narrowband FPC antennas). Indeed,

the knowledge of the leaky-mode wavenumber for the FPC antenna that is obtained by simulating only one periodic cell of the PRS over the ground plane is a useful tool for optimizing the bandwidth of wideband FPC antennas formed by a thick PRS. Importantly, all the formulas derived in this paper for wideband FPC antennas using electrically thick PRSs recover the formulas derived in the previous papers based on narrowband FPC antennas with thin PRSs.

Appendix A
Broadside Radiated Radiation Intensity Formula for an FPC Antenna Excited With a Magnetic Dipole

The broadside radiation intensity from an FPC antenna excited by a magnetic dipole moment ($I_m l$, where I_m is the magnetic current and l is its length) on the ground plane shown in Fig. 1(a) is calculated here. From reciprocity [53], the far-field electric field E_y at (or near) broadside from an FPC antenna excited by a magnetic dipole in the x-direction at $z = 0$ is related to the magnetic field H_x at the source location due to a testing electric dipole moment ($I_e l$) in the y-direction at a large distance $z = r = R+H$, where $z = H$ is the top of the (thick) PRS (the PRS has thickness $t = H - h$). In particular,

$$E_y(z = R + H) \times (I_e l) = -H_x(z = 0) \times (I_m l) \quad \text{(A1)}$$

where E_y represents the y-component of the electric field in the far-field zone ($z = R + H$) at a height R above the PRS due to the FPC antenna, and H_x is the x-component of the magnetic field at the magnetic dipole source location ($z = 0$), above the grand plane, due to the testing electric dipole in the far field. We first calculate the incident magnetic field at $z = H$ due to the testing electric dipole at a location $z = r$. The testing dipole launches a spherical wave that is locally a plane wave at top of the PRS ($z = H$) and given by

$$\mathbf{E} = \hat{\mathbf{y}}\, E_0(I_e l)\left(\frac{e^{-jk_0 R}}{R}\right) \quad \text{(A2)}$$

where $E_0 = -j\omega\mu_0/(4\pi)$ and because of the far-field, $R \approx r$. Then, the incident radiation intensity at the top of the PRS is calculated as [36], [37]

$$U^{\text{inc}} = \frac{|\mathbf{E}|^2}{2\eta_0} r^2 = \frac{|E_0|^2}{2\eta_0} |I_e l|^2. \quad \text{(A3)}$$

We model the thick PRS as a two-port network where port 1 is the connection between the transmission line and the top of the PRS and port 2 is the connection between the bottom of the PRS and the shorted transmission line as shown in Fig. 1(b). The power transmitted through the PRS is given by

$$U^{\text{trans}} = U^{\text{inc}} |S_{21}|^2. \quad \text{(A4)}$$

From reciprocity and conservation of energy for a lossless PRS, we have $S_{21} = S_{12}$ and $|S_{12}|^2 = 1 - |S_{22}|^2$, respectively, and in our case $S_{22} = \Gamma_{\text{PRS}}$. Formula (A4) is then written as

$$U^{\text{trans}} = U^{\text{inc}}(1 - |\Gamma_{\text{PRS}}|^2). \quad \text{(A5)}$$

The magnetic field transmitted through the PRS by the incident plane wave from the testing dipole is

$$H_x^{\text{trans}} = \sqrt{\xi_r}\sqrt{\frac{2U^{\text{trans}}}{\eta_0 r^2}} e^{j\phi^{\text{trans}}} \quad \text{(A6)}$$

where the phase term ϕ^{trans} accounts for the phase change of the wave going through the PRS. The transmitted magnetic field then bounces back and forth inside the cavity. Noting that the reflection coefficient for the magnetic field at the ground plane is $+1$, and the reflection coefficient for the magnetic field from the PRS is $-\Gamma_{\text{PRS}}$, the total magnetic field at the ground plane (where the magnetic dipole is) is represented (after summing a geometric series) as

$$H_x(0) = 2H_x^{\text{trans}} e^{-jk_{z1}h}\left(\frac{1}{1 + \Gamma_{\text{PRS}} e^{-j2k_{z1}h}}\right) \quad \text{(A7)}$$

where $k_{z1} = k_0\sqrt{\mu_r\varepsilon_r - \sin^2\theta}$. Combining formulas (A4) to (A7) results in

$$H_x(0) = 2\sqrt{\xi_r}\sqrt{\frac{2U^{\text{inc}}}{\eta_0 r^2}} e^{j(\phi^{\text{trans}} - k_{z1}h)}\left(\frac{\sqrt{(1 - |\Gamma_{\text{PRS}}|^2)}}{1 + \Gamma_{\text{PRS}} e^{-j2k_{z1}h}}\right). \quad \text{(A8)}$$

Then, applying the reciprocity relation (A1) into (A8), the far-field electric field is given as

$$E_y(r) = -2\sqrt{\xi_r}\sqrt{\frac{2U^{\text{inc}}}{\eta_0 r^2}}\left(\frac{I_m l}{I_e l}\right) e^{j(\phi^{\text{trans}} - k_{z1}h)} \times \left(\frac{\sqrt{(1 - |\Gamma_{\text{PRS}}|^2)}}{1 + \Gamma_{\text{PRS}} e^{-j2k_{z1}h}}\right). \quad \text{(A9)}$$

The radiation intensity near broadside generated by a magnetic dipole using the results from (A3) and (A9) is then given by

$$U(\omega, \theta) = \frac{|E_y|^2}{2\eta_0} r^2 = \frac{2\xi_r}{\eta_0^3} |E_0|^2 |I_m l|^2 \frac{(1 - |\Gamma_{\text{PRS}}|^2)}{|1 + \Gamma_{\text{PRS}} e^{-j2k_{z1}h}|^2}. \quad \text{(A10)}$$

This is formula (4) shown in Section II. To show the equivalence with the formula (3), we use

$$\Gamma_{\text{PRS}} = \frac{1 - (\bar{g} + j\bar{b})}{1 + (\bar{g} + j\bar{b})} \quad \text{(A11)}$$

where the conductance and susceptance looking up into the PRS from below, normalized to Y_1 (the intrinsic admittance of the substrate region), are

$$\bar{g} = g/Y_1, \quad \bar{b} = b/Y_1. \quad \text{(A12)}$$

After some algebra, we have from (A10) that

$$U(\omega, \theta) = \frac{\left(\frac{2\xi_r}{\eta_0^3}|E_0|^2|I_m l|^2\right)\frac{4\bar{g}}{(1+\bar{g})^2 + \bar{b}^2}}{\left(1 + \left(\frac{(1-\bar{g}) - j\bar{b}}{(1+\bar{g}) + j\,\bar{b}}\right) e^{-j2k_{z1}h}\right)\left(1 + \left(\frac{(1-\bar{g}) + j\bar{b}}{(1+\bar{g}) - j\,\bar{b}}\right) e^{+j2k_{z1}h}\right)}. \quad \text{(A13)}$$

We next use $e^{\pm j2k_{z1}h} = \cos(2k_{z1}h) \pm j\sin(2k_{z1}h)$ along with $\cos(2x) = \cos^2 x - \sin^2 x$, $\sin(2x) = 2\sin x \cos x$, with $x = k_{z1}h$. After some algebra, we arrive at

$$U(\omega,\theta) = \frac{2\xi_r}{\eta_0^3}|E_0|^2|I_m l|^2 \frac{\bar{g}}{(\cos x - \bar{b}\sin x)^2 + \bar{g}^2\sin^2 x} \tag{A14}$$

which is equivalent to formula (3).

Appendix B
Equivalency of Thin and Thick PRS Formulas

In this appendix, the equivalence of (15) and (19) is established for a narrowband FPC antenna operating over a narrow frequency range near the cavity resonance for broadside radiation.

A TEN model is considered as shown in Fig. 1(b), in which the admittance looking up into the PRS [given in (18)] is modeled as a shunt conductance g in parallel with a shunt susceptance b. We wish to then establish for this model that

$$\frac{-n_1 \ln|\Gamma_{\rm PRS}|}{(2k_0h)} = \frac{1}{2}n_1^2 \tan\delta_{\rm eff}. \tag{B1}$$

We assume a voltage on the transmission line inside the cavity that is taken as $\sin(k_1 z)$ for simplicity, where the wavenumber on the transmission line that models the cavity in the TEN is given by $k_1 = \omega_0\sqrt{(LC)}$, where L and C are the inductance and capacitance per unit length for the transmission line, and ω_0 is the frequency of operation, i.e., the resonance frequency of the structure. Following [54, eq. (2.37)], the power dissipated in this lossless transmission line by the load $(g + jb)$ is then given by

$$P_{\rm diss} = \frac{1}{2}|V_0^+|^2 Y_1(1 - |\Gamma_{\rm PRS}|^2) \tag{B2}$$

where $Y_1 = \sqrt{(C/L)}$. Next, we assume that the same transmission line has short circuits at both ends, corresponding to an ideal parallel-plate cavity region, and imagine the cavity has an effective loss tangent. The power dissipated in this lossy transmission line terminated by short circuits at both ends [54, eq. (2.94)] is given as

$$\begin{aligned} P_{\rm diss} &= \frac{|V_0^+|^2}{2Z_0}(2\sinh(GhZ_0)) \\ &\simeq |V_0^+|^2 Gh = |V_0^+|^2\omega_0 C(\tan\delta_{\rm eff})h. \end{aligned} \tag{B3}$$

Equating (B2) and (B3) shows that

$$Y_1(1 - |\Gamma_{\rm PRS}|^2) \simeq 2\omega_0 C(\tan\delta_{\rm eff})h. \tag{B4}$$

From Taylor approximation, we have

$$\ln|\Gamma_{\rm PRS}| = \frac{1}{2}\ln|\Gamma_{\rm PRS}|^2 \simeq -\frac{1}{2}(1 - |\Gamma_{\rm PRS}|^2). \tag{B5}$$

Inserting (B5) into (B4) and using $Y_1 = \sqrt{(C/L)}$, the resulting formula is identical to the one in (B1), after some simple algebra.

References

[1] G. Von Trentini, "Partially reflecting sheet arrays," *IRE Trans. Antennas Propag.*, vol. 4, no. 4, pp. 666–671, Oct. 1956.

[2] D. Jackson and N. Alexopoulos, "Gain enhancement methods for printed circuit antennas," *IEEE Trans. Antennas Propag.*, vol. 33, no. 9, pp. 976–987, Sep. 1985.

[3] D. R. Jackson and A. A. Oliner, "A leaky-wave analysis of the high-gain printed antenna configuration," *IEEE Trans. Antennas Propag.*, vol. 36, no. 7, pp. 905–910, Jul. 1988.

[4] D. R. Jackson *et al.*, "The fundamental physics of directive beaming at microwave and optical frequencies and the role of leaky waves," *Proc. IEEE*, vol. 99, no. 10, pp. 1780–1805, Oct. 2011.

[5] D. R. Jackson, C. Caloz, and T. Itoh, "Leaky-wave antennas," *Proc. IEEE*, vol. 100, no. 7, pp. 2194–2206, Jul. 2012.

[6] A. T. Almutawa, H. Kazemi, and F. Capolino, "Analyze and design of thin planar high impedance surface as an antenna," in *Proc. Int. Conf. Electromagn. Adv. Appl. (ICEAA)*, 2018, pp. 623–624.

[7] S. Sengupta, D. R. Jackson, A. T. Almutawa, H. Kazemi, F. Capolino, and S. A. Long, "Radiation properties of a 2D periodic leaky-wave antenna," *IEEE Trans. Antennas Propag.*, vol. 67, no. 6, pp. 3560–3573, Jun. 2019.

[8] T. Zhao, D. R. Jackson, J. T. Williams, and A. A. Oliner, "General formulas for 2-D leaky-wave antennas," *IEEE Trans. Antennas Propag.*, vol. 53, no. 11, pp. 3525–3533, Nov. 2005.

[9] T. Zhao, D. R. Jackson, J. T. Williams, H.-Y. D. Yang, and A. A. Oliner, "2-D periodic leaky-wave antennas—Part I: Metal patch design," *IEEE Trans. Antennas Propag.*, vol. 53, no. 11, pp. 3505–3514, Nov. 2005.

[10] T. Zhao, D. R. Jackson, and J. T. Williams, "2-D periodic leaky-wave antennas—Part II: Slot design," *IEEE Trans. Antennas Propag.*, vol. 53, no. 11, pp. 3515–3524, Nov. 2005.

[11] R. Gardelli, M. Albani, and F. Capolino, "Array thinning by using antennas in a Fabry–Pérot cavity for gain enhancement," *IEEE Trans. Antennas Propag.*, vol. 54, no. 7, pp. 1979–1990, Jul. 2006.

[12] G. Lovat, P. Burghignoli, and D. R. Jackson, "Fundamental properties and optimization of broadside radiation from uniform leaky-wave antennas," *IEEE Trans. Antennas Propag.*, vol. 54, no. 5, pp. 1442–1452, May 2006.

[13] G. Lovat, P. Burghignoli, F. Capolino, and D. R. Jackson, "Highly-directive planar leaky-wave antennas: A comparison between metamaterial-based and conventional designs," in *Proc. Eur. Microw. Assoc.*, vol. 12, 2006, p. 21.

[14] P. Burghignoli, G. Lovat, F. Capolino, D. R. Jackson, and D. R. Wilton, "Highly polarized, directive radiation from a Fabry–Pérot cavity leaky-wave antenna based on a metal strip grating," *IEEE Trans. Antennas Propag.*, vol. 58, no. 12, pp. 3873–3883, Dec. 2010.

[15] F. De Flaviis, A. Hosseini, and F. Capolino, "A 60 GHz simple-to-fabricate single-layer planar Fabry–Pérot cavity antenna," *IET Microw. Antennas Propag.*, vol. 9, no. 4, pp. 313–318, Mar. 2015.

[16] A. Hosseini, A. T. Almutawa, F. Capolino, and D. R. Jackson, "Wideband single-layer Fabry–Pérot cavity antenna with a radial variation of the cavity permittivity," in *Proc. IEEE Int. Symp. Antennas Propag., USNC/URSI Nat. Radio Sci. Meeting*, Jul. 2017, pp. 2659–2660.

[17] A. Hosseini, F. De Flaviis, and F. Capolino, "Design formulas for planar Fabry–Pérot cavity antennas formed by thick partially reflective surfaces," *IEEE Trans. Antennas Propag.*, vol. 64, no. 12, pp. 5487–5491, Dec. 2016.

[18] S. A. Hosseini, F. Capolino, and F. De Flaviis, "Q-band single-layer planar Fabry–Pérot cavity antenna with single integrated-feed," *Prog. Electromagn. Res. C*, vol. 52, pp. 135–144, Aug. 2014.

[19] S. A. Hosseini, F. Capolino, and F. De Flaviis, "A new formula for the pattern bandwidth of Fabry–Pérot cavity antennas covered by thin frequency selective surfaces," *IEEE Trans. Antennas Propag.*, vol. 59, no. 7, pp. 2724–2727, Jul. 2011.

[20] A. Hosseini, F. Capolino, F. De Flaviis, P. Burghignoli, G. Lovat, and D. R. Jackson, "Improved bandwidth formulas for Fabry–Pérot cavity antennas formed by using a thin partially-reflective surface," *IEEE Trans. Antennas Propag.*, vol. 62, no. 5, pp. 2361–2367, May 2014.

[21] A. P. Feresidis and J. C. Vardaxoglou, "High gain planar antenna using optimised partially reflective surfaces," *IEE Proc.-Microw., Antennas Propag.*, vol. 148, no. 6, pp. 345–350, Dec. 2001.

[22] A. P. Feresidis and J. C. Vardaxoglou, "A broadband high-gain resonant cavity antenna with single feed," in *Proc. 1st Eur. Conf. Antennas Propag. (EuCAP)*, 2006, pp. 1–5.

[23] L. Moustafa and B. Jecko, "EBG structure with wide defect band for broadband cavity antenna applications," *IEEE Antennas Wireless Propag. Lett.*, vol. 7, pp. 693–696, 2008.

[24] Y.-F. Lu and Y.-C. Lin, "Design and implementation of broadband partially reflective surface antenna," in *Proc. IEEE Int. Symp. Antennas Propag. (APSURSI)*, Jul. 2011, pp. 2250–2253.

[25] C. Mateo-Segura, A. P. Feresidis, and G. Goussetis, "Broadband leaky-wave antennas with double-layer PRS: Analysis and design," in *Proc. 5th Eur. Conf. Antennas Propag. (EUCAP)*, 2011, pp. 2102–2105.

[26] Y. Ge, K. P. Esselle, and T. S. Bird, "The use of simple thin partially reflective surfaces with positive reflection phase gradients to design wideband, low-profile EBG resonator antennas," *IEEE Trans. Antennas Propag.*, vol. 60, no. 2, pp. 743–750, Feb. 2012.

[27] D. Kim, J. Ju, and J. Choi, "A mobile communication base station antenna using a genetic algorithm based Fabry–Pérot resonance optimization," *IEEE Trans. Antennas Propag.*, vol. 60, no. 2, pp. 1053–1058, Feb. 2012.

[28] M. A. Al-Tarifi, D. E. Anagnostou, A. K. Amert, and K. W. Whites, "Bandwidth enhancement of the resonant cavity antenna by using two dielectric superstrates," *IEEE Trans. Antennas Propag.*, vol. 61, no. 4, pp. 1898–1908, Apr. 2013.

[29] K. Konstantinidis, K. P. Feresidis, and P. S. Hall, "Multilayer partially reflective surfaces for broadband Fabry–Pérot cavity antennas," *IEEE Trans. Antennas Propag.*, vol. 62, no. 7, pp. 3474–3481, Jul. 2014.

[30] C. Mateo-Segura, A. P. Feresidis, and G. Goussetis, "Bandwidth enhancement of 2-D leaky-wave antennas with double-layer periodic surfaces," *IEEE Trans. Antennas Propag.*, vol. 62, no. 2, pp. 586–593, Feb. 2014.

[31] A. Hosseini, F. Capolino, and D. R. Jackson, "Leaky-wave explanation of gain-bandwidth-enhanced Fabry–Pérot cavity antennas formed by a thick multilayer partially-reflective surface," in *Proc. IEEE Int. Symp. Antennas Propag., USNC/URSI Nat. Radio Sci. Meeting*, Jul. 2015, pp. 1090–1091.

[32] K. Konstantinidis, A. P. Feresidis, and P. S. Hall, "Broadband sub-wavelength profile high-gain antennas based on multi-layer metasurfaces," *IEEE Trans. Antennas Propag.*, vol. 63, no. 1, pp. 423–427, Jan. 2015.

[33] N. Wang, J. Li, G. Wei, L. Talbi, Q. Zeng, and J. Xu, "Wideband Fabry–Pérot resonator antenna with two layers of dielectric superstrates," *IEEE Antennas Wireless Propag. Lett.*, vol. 14, pp. 229–232, 2015.

[34] A. Hosseini, A. T. Almutawa, F. Capolino, and D. R. Jackson, "V-band wideband Fabry–Pérot cavity antenna made of thick partially-reflective surface," in *Proc. IEEE Int. Symp. Antennas Propag. (APSURSI)*, Jun./Jul. 2016, pp. 349–350.

[35] Y. Ge and K. P. Esselle, "A method to design dual-band, high-directivity EBG resonator antennas using single-resonant, single-layer partially reflective surfaces," *Prog. Electromagn. Res. C*, vol. 13, pp. 245–257, 2010.

[36] W. L. Stutzman and G. A. Thiele, *Antenna Theory and Design*, 3rd ed. Hoboken, NJ, USA: Wiley, 2012.

[37] C. A. Balanis, *Antenna Theory: Analysis and Design*, 4th ed. Hoboken, NJ, USA: Wiley, 2015.

[38] L. B. Felsen and N. Marcuvitz, *Radiation and Scattering of Waves*, vol. 31. Hoboken, NJ, USA: Wiley, 1994.

[39] A. Ip and D. R. Jackson, "Radiation from cylindrical leaky waves," *IEEE Trans. Antennas Propag.*, vol. 38, no. 4, pp. 482–488, Apr. 1990.

[40] H. Mirzaei and G. V. Eleftheriades, "Realizing non-Foster reactive elements using negative-group-delay networks," *IEEE Trans. Microw. Theory Techn.*, vol. 61, no. 12, pp. 4322–4332, Dec. 2013.

[41] G. Lovat, P. Burghignoli, F. Capolino, D. R. Jackson, and D. R. Wilton, "Analysis of directive radiation from a line source in a metamaterial slab with low permittivity," *IEEE Trans. Antennas Propag.*, vol. 54, no. 3, pp. 1017–1030, Mar. 2006.

[42] D. R. Jackson, A. A. Oliner, and A. Ip, "Leaky-wave propagation and radiation for a narrow-beam multiple-layer dielectric structure," *IEEE Trans. Antennas Propag.*, vol. 41, no. 3, pp. 344–348, Mar. 1993.

[43] A. Hosseini, F. Capolino, and F. De Flaviis, "Gain enhancement of a V-band antenna using a Fabry–Pérot cavity with a self-sustained all-metal cap with FSS," *IEEE Trans. Antennas Propag.*, vol. 63, no. 3, pp. 909–921, Mar. 2015.

[44] J. L. Gómez-Tornero, A. Martínez-Ros, A. Álvarez-Melcón, F. Mesa, and F. Medina, "Substrate integrated waveguide leaky-wave antenna with reduced beam squint," in *Proc. Eur. Microw. Conf.*, 2013, pp. 491–494.

[45] J. L. Gómez-Tornero, M. Poveda-García, R. Guzmán-Quirós, and D. Cañete-Rebenaque, "Reducing the beam squint in scanned leaky-wave antennas using coupled SIW cavities," in *Proc. IEEE Int. Symp. Antennas Propag. (APSURSI)*, Jun./Jul. 2016, pp. 77–78.

[46] M. Poveda-García, D. Cañete-Rebenaque, G. Goussetis, and J. L. Gómez-Tornero, "Coupling substrate-integrated waveguides to increase the gain bandwidth of leaky-wave antennas," *IEEE Trans. Microw. Theory Techn.*, vol. 66, no. 6, pp. 3099–3109, Jun. 2018.

[47] M. Poveda-García, R. Guzmán-Quirós, S. Rottenberg, J. L. Gómez-Tornero, C. Mateo-Segura, and G. Goussetis, "Anomalous leaky-mode dispersion of coupled-cavity wideband leaky-wave antennas," in *Proc. 12th Eur. Conf. Antennas Propag. (EuCAP)*, 2018, pp. 1–5.

[48] V. R. Komanduri, D. R. Jackson, and S. A. Long, "Radiation characteristics of finite-length 1D-uniform leaky wave antennas radiating at broadside," in *Proc. IEEE Antennas Propag. Soc. Int. Symp.*, Jul. 2010, pp. 1–4.

[49] *Ansys-HFSS User Guide, Version 19*, ANSYS, Canonsburg, PA, USA, 2017.

[50] M. García-Vigueras, P. De Lara-Guarch, J. L. Gómez-Tornero, R. Guzmán-Quirós, and G. Goussetis, "Efficiently illuminated broadside-directed 1D and 2D tapered Fabry–Pérot leaky-wave antennas," in *Proc. 6th Eur. Conf. Antennas Propag. (EUCAP)*, 2012, pp. 247–251.

[51] M. A. Al-Tarifi, A. K. Amert, D. E. Anagnostou, and K. W. Whites, "Application of a dielectric puck for a high gain-bandwidth resonant cavity antenna," in *Proc. IEEE Int. Symp. Antennas Propag.*, Jul. 2012, pp. 1–2.

[52] R. M. Hashmi, B. A. Zeb, and K. P. Esselle, "Wideband high-gain EBG resonator antennas with small footprints and all-dielectric superstructures," *IEEE Trans. Antennas Propag.*, vol. 62, no. 6, pp. 2970–2977, Jun. 2014.

[53] R. F. Harrington, *Time-Harmonic Electromagnetic Fields*. New York, NY, USA: Wiley, 2001.

[54] D. M. Pozar, *Microwave Engineering*, 4th ed. Hoboken, NJ, USA: Wiley, 2012.

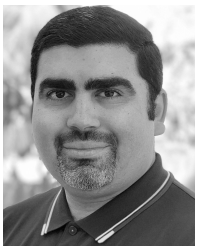

Ahmad T. Almutawa (S'05–M'06) was born in Kuwait, in 1984. He received the B.S. and M.S. degrees in electrical engineering from Kuwait University, Kuwait, in 2006 and 2009, respectively, and the M.S. degree in electrical engineering (wireless circuits and systems) from the University of South Florida, Tampa, FL, USA, in 2011. He is currently pursuing the Ph.D. degree in electrical engineering (electromagnetics and meta-materials) with the University of California, Irvine, CA, USA.

Since 2011, he has been a Faculty Member with the Electronic Engineering Technology Department, Public Authority for Applied Education and Training, Kuwait. His current research interests include leaky-wave antennas and metamaterial-based antennas.

Alister Hosseini (S'08–M'14) received the B.S. degree in electrical engineering (electronics: analog IC design and digital electronics: DSPs, microprocessors and microcontrollers) from the Sharif University of Technology, Tehran, Iran, the M.S. degree in electrical engineering (optimization and numerical methods in electromagnetics, ultrawideband antennas, and metamaterial-based microwave circuits) from Tarbiat Modares University, Tehran, and the Ph.D. degree in electrical engineering (electromagnetics, reconfigurable antennas and circuits, and millimeter-wave Fabry–Pérot cavity antennas) from the University of California, Irvine, CA, USA.

He received the Henry Samueli and Holmes Fellowships during his doctoral research at UC Irvine. His current research interests include novel Fabry–Pérot cavity antennas, on-chip MMW antennas, RFID antennas and circuits, RF energy-harvesting systems, active reflectarrays, reconfigurable antennas and circuits, and metamaterial antennas and circuits. He has authored or coauthored more than 35 papers in reference journals and conference proceedings and filed over 40 utility patents (over 15 granted patents). He has coauthored the chapter "Electromagnetic Metamaterials as Artificial Composite Structures" in *Handbook of Nanoscience, Engineering and Technology* (CRC Press, 2012).

Dr. Hosseini is currently a Technical Fellow in industry responsible for various cutting-edge projects.

David R. Jackson (F'99) was born in St. Louis, MO, USA, in 1957. He received the B.S.E.E. and M.S.E.E. degrees from the University of Missouri, Columbia, MO, USA, in 1979 and 1981, respectively, and the Ph.D. degree in electrical engineering from the University of California, Los Angeles, CA, USA, in 1985.

From 1985 to 1991, he was an Assistant Professor with the Department of Electrical and Computer Engineering, University of Houston, Houston, TX, USA, where he was an Associate Professor from 1991 to 1998 and has been a Professor since 1998. His current research interests include microstrip antennas and circuits, leaky-wave antennas, leakage and radiation effects in microwave integrated circuits, periodic structures, and electromagnetic compatibility and interference.

Dr. Jackson is currently serving as the Immediate Past Chair of USNC-URSI, the U.S. National Committee (USNC) for URSI, and the International Union of Radio Science. From 2015 to 2018, he served as the Chair of USNC-URSI. He is also on the Education Committee of the Antennas and Propagation Society (AP-S) and on the MTT-15 (Microwave Field Theory) Technical Committee of the Microwave Theory and Techniques Society. He has been the Chair of the Distinguished Lecturer Committee of the IEEE Antennas and Propagation Society (AP-S), the Transnational Committee of the IEEE AP-S, the Chapter Activities Committee of the AP-S, and has been a Distinguished Lecturer for the AP-S, a member of the AdCom for the AP-S, and an Associate Editor of the IEEE TRANSACTIONS ON ANTENNAS AND PROPAGATION, the *International Journal of RF*, and the *Microwave Computer-Aided Engineering*. He served as the Chair of the MTT-15 (Microwave Field Theory) Technical Committee. He also served as the Chair of Commission B of USNC-URSI and as the Secretary of this Commission.

Filippo Capolino (S'94–M'97–SM'04) received the Laurea (*cum laude*) and Ph.D. degrees in electrical engineering from the University of Florence, Florence, Italy, in 1993 and 1997, respectively.

He was an Assistant Professor with the Department of Information Engineering, University of Siena, Siena, Italy, until 2002. From 1997 to 1999, he was a Fulbright and then a Post-Doctoral Fellow with the Department of Aerospace and Mechanical Engineering, Boston University, Boston, MA, USA. From 2000 to 2001, part of 2005 and in 2006, he was a Research Assistant Visiting Professor with the Department of Electrical and Computer Engineering, University of Houston, Houston, TX, USA. He has been a Visiting Professor with the Fresnel Institute, Marseille, France, since 2003, and with the Centre de Recherche Paul Pascal, Bordeaux, France, since 2010. He is currently a Professor with the Department of Electrical Engineering and Computer Science, University of California, Irvine, CA, USA. His current research interests include metamaterials and their applications, traveling wave tubes, antennas, sensors in both microwave and optical ranges, plasmonics, microscopy, wireless systems, millimeter wave chip-integrated antennas, and applied electromagnetics in general.

Dr. Capolino was a recipient of the R. W. P. King Prize Paper Award from the IEEE Antennas and Propagation Society for the Best Paper of the Year 2000, by an author under 36. He was the EU Coordinator of the EU Doctoral Programs on Metamaterials from 2004 to 2009. From 2002 to 2008, he served as an Associate Editor for the IEEE TRANSACTIONS ON ANTENNAS AND PROPAGATION. He is the Editor of the *Metamaterials Handbook* (Boca Raton, FL, USA: CRC Press, 2009).